Journal of Magnetic Resonance 211 (2011) 162–169

Contents lists available at ScienceDirect

Journal of Magnetic Resonance

journal homepage: www.elsevier.com/locate/jmr

Fast high-resolution 2D correlation spectroscopy in inhomogeneous fields via Hadamard intermolecular multiple quantum coherences technique

Congbo Cai, Fenglian Gao, Shuhui Cai, Yuqing Huang, Zhong Chen *

Departments of Electronic Science and Communication Engineering, Fujian Key Laboratory of Plasma and Magnetic Resonance, State Key Laboratory for Physical Chemistry of Solid Surfaces, Xiamen University, Xiamen 361005, PR China

ARTICLE INFO

Article history:
Received 27 January 2011
Revised 15 April 2011
Available online 23 May 2011

Keywords:
Intermolecular multiple quantum coherence
Hadamard
COSY
High-resolution spectra
Inhomogeneous field

ABSTRACT

Recently, a method based on intermolecular multiple quantum coherences (iMQCs) has been proposed to obtain high-resolution 2D COSY spectra in inhomogeneous fields via 3D acquisitions. However, the very long acquisition time prevents its practical application. To overcome this shortage, the Hadamard technique was applied for the iMQC method in this paper. For the new pulse sequence, the direct frequency-domain excitation is used in the first indirect detection dimension, so the 3D acquisition was replaced by an array of 2D acquisitions. The acquisition time can be reduced to 10 min. The resulting spectra retain useful structural information including chemical shifts and multiplet patterns of *J* coupling even when the inhomogeneous line broadening leads to overlap of neighboring diagonal resonances in the conventional COSY spectrum. The experimental results are consistent with the theoretical predictions and computer simulations. The new sequence may provide a time-efficient way for the studies of chemical solution in inhomogeneous fields.

1. Introduction

High-resolution 2D homonuclear correlation spectroscopy (COSY) contains useful information such as chemical shifts, scalar coupling constants, and multiplet patterns, and capable of analyzing molecular structures and compositions [1,2]. It has found many applications since its establishment [3]. However, the homogeneity of magnetic field of the order of 10^{-8} over the sample volume is usually required for a high-resolution ^{1}H–1H COSY spectrum. This cannot be satisfied in some circumstances [4,5], which results in broadened linewidth and low spectral resolution. Consequently, much spectral information would be lost, such as scalar coupling constants and multiplet patterns.

Intermolecular multiple quantum coherences (iMQCs) possess interesting properties [6–8]. One of the attractive properties is that they can be used to encode material geometry over intermediate length scales, no matter it is contained inside an imaging voxel or buried in the total signal [9]. This unique property has been utilized to provide distance-selected contrast sensitive to differences in resonance frequency and magnetization density [10,11]. It can also be applied for *in vivo* high-resolution NMR spectra [12–14]. Compared to a conventional spectrum in which the linewidth is determined by the homogeneity of a magnetic field across the sample, the linewidth in a high-resolution 1D iMQC spectrum generally results from the relative homogeneity of a magnetic field within the dipolar correlation distance [15,16].

Recently, one iMQC method was proposed to obtain high-resolution COSY spectra in inhomogeneous fields via 3D acquisition [17,18]. The acquisition time is generally more than several hours, which is a great obstacle for its application in time-concerned studies, such as in the study of dynamic process. For a 2D COSY spectrum, numerous t_1 increments are required for good resolution. An alternative way for fast acquiring 2D COSY spectrum is based on the Hadamard encoding and decoding technique [19]. The basic strategy is only exciting the signal-bearing areas in the indirect detection dimension with soft polychromatic excitation pulses encoded by a Hadamard matrix with order *N*. Then the number of t_1 increments needed for a conventional high-resolution COSY spectrum is replaced by a relative small number *N*, and the evolution period t_1 in every scan is also replaced by a constant duration τ. This technique greatly benefits to the scanning time [20].

In this paper, the Hadamard technique was introduced to the intermolecular dipolar-interaction enhanced all lines II (IDEAL-II) sequence for the high-resolution COSY spectra in inhomogeneous fields with time-efficient acquisition [21]. In the new sequence named Hadamard-IDEAL-II, soft polychromatic excitation pulse with Hadamard encoding is used to excite the desired chemical shift sites. Acquisition using this sequence in inhomogeneous fields provides data, which can give high-resolution 2D COSY spectra after Hadamard decoding. In the following, detail theoretical analysis, experimental and simulation results are given.

* Corresponding author. Fax: +86 592 2189426.
E-mail address: chenz@xmu.edu.cn (Z. Chen).

1090-7807/$ - see front matter © 2011 Elsevier Inc. All rights reserved.
doi:10.1016/j.jmr.2011.05.008

2. Theoretical formalism

2.1. Hadamard encoding and decoding

The Hadamard technique has been used to shorten the acquisition time for 2D or multidimensional NMR spectra [22]. Assume N soft polychromatic pulses are necessary to excite all desired frequency sites, there is a corresponding Hadamard matrix with order N. The N satisfies either the relationship $N = 2^k$ or the relationship $N = 4k$, where k is an integer. Based on the method for producing multiple-frequency-shifted laminar pulses [23], the amplitude of individual frequency component can be controlled separately without difficulty. Given the amplitude of each frequency component is encoded according to a row of Hadamard matrix, where '+1' represents the frequency component with positive amplitude and '−1' represents the frequency component with negative amplitude, N soft polychromatic pulses can be constructed easily, which can excite multiple frequency sites simultaneously. Since the number of frequency sites (M) is smaller than the order of Hadamard matrix (N), some of the channels are not used and set *NULL*. After N scans with soft polychromatic pulses, there will be N composited free induction decay signals from all frequency sites. Followed with Hadamard decoding, the signals from M frequency-sites are decoded separately, and the signals from *NULL* are discarded [24].

2.2. High-resolution COSY by Hadamard technique

The schematic diagram of the Hadamard-IDEAL-II high-resolution COSY method is shown in Fig. 1. It is noted that if the signal-bearing areas are overlapped due to large field inhomogeneities, a 1D high-resolution spectrum obtained from the IDEAL-II sequence should be used to determine the number of frequency sites (M) and their frequency values. According to the number M and the frequency-shifts of the frequency-sites, the soft polychromatic pulses can be produced as described above with a Hadamard matrix of order N ($N > M$). After N scans and Hadamard decoding, a set of 2D spectra can be obtained. Rotating these decoded spectra and projecting them onto the F2 dimension, there would be N 1D high-resolution spectra running in the F2 dimension which include all correlation information for reconstructing a high-resolution COSY spectrum. The Hadamard-IDEAL-II sequence is shown in Fig. 2. In the sequence, the first pulse is a soft polychromatic pulse and the third one is selective only for the solvent spin. J coupling takes effect after the soft polychromatic pulse. Three linear coherence selection gradients (CSGs) are used to select the coherence transfer pathway $0 \rightarrow +2 \rightarrow -1$. The first CSG should be large enough to dephase all the coherence orders except intermolecular zero-quantum coherences (iZQCs) which are free of the inhomogeneities in the evolution period τ, while the second and third CSGs have a ratio of 1:2 in the strength with a same duration in order

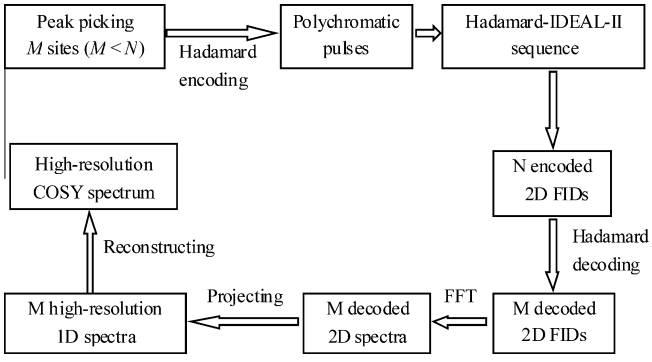

Fig. 1. Schematic diagram for the 2D high-resolution Hadamard COSY spectroscopy.

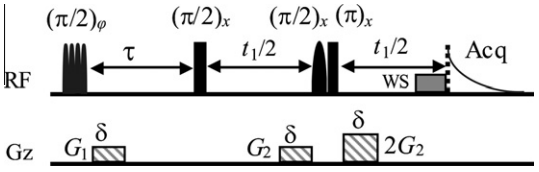

Fig. 2. Hadamard-IDEAL-II sequence. The first selective soft pulse is a polychromatic excitation pulse capable of exciting all interested signal-loading areas. The second selective pulse with gauss-shape is only selective for solvent spin. The "WS" module is for water suppression.

to select the intermolecular double-quantum coherences (iDQCs). In addition, the water suppression (WS) module is involved to suppress the solvent signal [25].

In the following discussion, the distant dipolar field (DDF) theory combined with product operator formalism is used to deduce the analytical expression of signals from the new sequence [26–30]. For simplicity, the sample is assumed to be a homogeneous liquid mixture consisting of two isolated spins (I_1 and I_2) and an AX spin-1/2 system which includes two spins (S_k and S_l) with a scalar coupling constant J_{kl}. I_1 is solvent, and I_2 and S are solute. ω_m is the frequency offset of spin m ($m = I_1, I_2, S_k, S_l$) in the rotating frame. P_1, P_2, P_3, and P_4 are the positive or negative signs of individual frequency components (I_1, I_2, S_k, S_l) in a soft polychromatic pulse.

For simplification, the effects of radiation damping, diffusion, relaxation, and intermolecular NOE are ignored and the inhomogeneity of background field is only along the Z axis. When the magnetization is fully modulated and varies only in one direction, the dipolar field is localized and an exact theoretical expression for the iMQC signals can be deduced [31]. For the spin system discussed, the reduced density operators $\sigma_{eq}^{I_1}, \sigma_{eq}^{I_2}$ for I_1, I_2 protons and σ_{eq}^{S} for S protons at initial thermal equilibrium state with the high-temperature approximation can be given by

$$\begin{aligned} \sigma_{eq}^{I_1} &= I_{1z} \\ \sigma_{eq}^{I_2} &= I_{2z} \\ \sigma_{eq}^{S} &= S_{kz} + S_{lz} \end{aligned} \tag{1}$$

where the Boltzmann factor has been omitted for clarity; I_{1z}, I_{2z}, S_{kz}, and S_{lz} represent the longitudinal components of I_1, I_2, S_k and S_l spins, respectively. Since S_k is similar to S_l in an AX spin-1/2 system, we only deduced the density operators evolution starting from S_k.

In the new sequence, the soft polychromatic pulse rotates the spin magnetizations into the transverse plane. The transverse magnetizations of different frequency sites have different phases (X or $-X$ direction) which are determined by the every row of Hadamard matrix, where the signs of '+' and '−' (represented by P_1, P_2, P_3, and P_4 for the frequency components of I_1, I_2, S_k, and S_l correspondingly) indicate the positive and negative phases respectively. During the first evolution period τ, the spins evolve under chemical shifts, J couplings, field inhomogeneities, and the first gradient pulse. Just before the second non-selective $(\pi/2)_x$ RF pulse, the state of the spin system at position z and time τ can be described by the reduced density operators $\sigma^{I_1}(\tau^-, z), \sigma^{S_k}(\tau^-, z)$ and $\sigma^{I_2}(\tau^-, z)$,

$$\begin{aligned} \sigma^{I_1}(\tau^-, z) &= -P_1 I_{1y}\cos(H_1) + P_1 I_{1x}\sin(H_1) \\ \sigma^{I_2}(\tau^-, z) &= -P_2 I_{2y}\cos(H_2) + P_2 I_{2x}\sin(H_2) \\ \sigma^{S_k}(\tau^-, z) &= -P_3\{S_{ky}\cos(H_3) - S_{kx}\sin(H_3)\}\cos(\pi J_{kl}\tau) \\ &\quad + P_3\{2S_{kx}S_{lz}\cos(H_3) + 2S_{ky}S_{lz}\sin(H_3)\}\sin(\pi J_{kl}\tau) \end{aligned} \tag{2}$$

where $\begin{cases} H_1 = \omega_{I_1}\tau + \gamma\Delta B(z)\tau + \gamma G_1\delta z \\ H_2 = \omega_{I_2}\tau + \gamma\Delta B(z)\tau + \gamma G_1\delta z \\ H_3 = \omega_{S_k}\tau + \gamma\Delta B(z)\tau + \gamma G_1\delta z \end{cases}$, γ is the gyromagenatic ratio, G_1 and δ are strength and duration of the first CSG, respectively. $\Delta B(z)$ is the field inhomogeneity at position z. Immediately after the first non-selective $(\pi/2)_x$ RF pulse, we have

$$\begin{aligned}\sigma^{I_1}(\tau,z) &= -P_1 I_{1z}\cos(H_1) + P_1 I_{1x}\sin(H_1)\\ \sigma^{I_2}(\tau,z) &= -P_2 I_{2z}\cos(H_2) + P_2 I_{2x}\sin(H_2)\\ \sigma^{S_k}(\tau,z) &= -P_3\{S_{kz}\cos(H_3) - S_{ky}\sin(H_3)\}\cos(\pi J_{kl}\tau)\\ &\quad + P_3\{-2S_{kx}S_{ly}\cos(H_3) - 2S_{kz}S_{ly}\sin(H_3)\}\sin(\pi J_{kl}\tau)\end{aligned} \tag{3}$$

Though the density operators $\sigma^{I_1}(\tau,z)$, $\sigma^{I_2}(\tau,z)$ and $\sigma^{S_k}(\tau,z)$ all contain spatially modulated longitudinal magnetization component, only I_1 spin can produce effective DDF. This is because that I_2 and S_k spins are only excited by the first and second RF pulses in the sequence, so they can produce effective DDFs only when the condition $-G_2\delta = nG_1\delta$ is fulfilled, where n is an integer [17]. The condition $-G_2\delta = nG_1\delta$ is easily broken by the setting of G_1 and G_2 parameters in experiments. According to the DDF theory, when the CSGs are along the Z direction, $B_d^{I_1}(z)$, $B_d^{I_2}(z)$ and $B_d^{S}(z)$, which represent the DDFs experienced by I_1, I_2 and S_k at position z, can be described as follows:

$$\begin{aligned}B_d^{I_1}(z) &= -\frac{1}{\gamma\tau_d}P_1\cos(H_1)\\ B_d^{I_2}(z) &= -\frac{2}{3\gamma\tau_d}P_1\cos(H_1)\\ B_d^{S}(z) &= -\frac{2}{3\gamma\tau_d}P_1\cos(H_1)\end{aligned} \tag{4}$$

where $\tau_d = \left(\gamma\mu_0 M_0^{I_1}\right)^{-1}$ is the dipolar demagnetizing time of I_1 spin, in which μ_0 is vacuum magnetic permeability and $M_0^{I_1}$ is the equilibrium magnetization intensity of I_1 spin. In the following, $B_d^{I_1}(z)$, $B_d^{I_2}(z)$ and $B_d^{S}(z)$ are written as $B_d^{I_1}$, $B_d^{I_2}$ and B_d^{S} for short. After the first non-selective $(\pi/2)_x$ RF pulse, the spins evolve during the first $t_1/2$ period. We have

$$\begin{aligned}\sigma^{I_1}(\tau+t_1^-/2,z) &= P_1 I_{1x}\cos(H_4)\sin(H_1) + P_1 I_{1y}\sin(H_4)\sin(H_1) - P_1 I_{1z}\cos(H_1)\\ \sigma^{I_2}(\tau+t_1^-/2,z) &= P_2 I_{2x}\cos(H_5)\sin(H_2) + P_2 I_{2y}\sin(H_5)\sin(H_2) - P_2 I_{2z}\cos(H_2)\\ \sigma^{S_k}(\tau+t_1^-/2,z) &= -P_3 S_{kz}\cos(H_3)\cos(\pi J_{kl}\tau)\\ &\quad + P_3 S_{ky}A_1\cos(\pi J_{kl}t_1/2)\cos(\pi J_{kl}\tau)\\ &\quad - 2P_3 S_{kx}S_{lz}A_1\sin(\pi J_{kl}t_1/2)\cos(iJ_{kl}\tau)\\ &\quad - P_3 S_{kx}A_2\cos(\pi J_{kl}t_1/2)\cos(\pi J_{kl}\tau)\\ &\quad - 2P_3 S_{ky}S_{lz}A_2\sin(\pi J_{kl}t_1/2)\cos(\pi J_{kl}\tau)\\ &\quad + 2P_3 S_{kz}S_{lx}A_4\cos(\pi J_{kl}t_1/2)\sin(\pi J_{kl}\tau)\\ &\quad + P_3 S_{ly}A_4\sin(\pi J_{kl}t_1/2)\sin(\pi J_{kl}\tau)\\ &\quad - 2P_3 S_{kz}S_{ly}A_3\cos(\pi J_{kl}t_1/2)\sin(\pi J_{kl}\tau)\\ &\quad + P_3 S_{lx}A_3\sin(\pi J_{kl}t_1/2)\sin(\pi J_{kl}\tau)\end{aligned} \tag{5}$$

where $\begin{cases}H_4 = (\omega_{I_1} + \gamma\Delta B(z) + \gamma B_d^{I_1})t_1/2 + \gamma G_2\delta z\\ H_5 = (\omega_{I_2} + \gamma\Delta B(z) + \gamma B_d^{I_2})t_1/2 + \gamma G_2\delta z\\ H_6 = (\omega_{S_l} + \gamma\Delta B(z) + \gamma B_d^{S})t_1/2 + \gamma G_2\delta z\end{cases}$, and

$\begin{cases}A_1 = \cos(H_6)\sin(H_3)\\ A_2 = \sin(H_6)\sin(H_3)\\ A_3 = \cos(H_6)\sin(H_3)\\ A_4 = \sin(H_6)\sin(H_3)\end{cases}$.

After the selective $(\pi/2)_x^{I_1}$ RF pulse which only acts on the spin I_1 and the non-selective $(\pi)_x$ RF pulse, we have

$$\begin{aligned}\sigma^{I_1}(\tau+t_1/2,z) &= -P_1 I_{1z}\sin(H_4)\sin(H_1) + P_1 I_{1x}\cos(H_4)\sin(H_1)\\ &\quad - P_1 I_{1y}\cos(H_1)\\ \sigma^{I_2}(\tau+t_1/2,z) &= P_2 I_{2z}\cos(H_2) + P_2 I_{2x}\cos(H_5)\sin(H_2)\\ &\quad - P_2 I_{2y}\sin(H_5)\sin(H_2)\\ \sigma^{S_k}(\tau+t_1/2,z) &= P_3 S_{kz}\cos(H_3)\cos(\pi J_{kl}\tau)\\ &\quad - P_3 S_{ky}A_1\cos(\pi J_{kl}t_1/2)\cos(\pi J_{kl}\tau)\\ &\quad + 2P_3 S_{kx}S_{lz}A_1\sin(\pi J_{kl}t_1/2)\cos(iJ_{kl}\tau)\\ &\quad - P_3 S_{kx}A_2\cos(\pi J_{kl}t_1/2)\cos(\pi J_{kl}\tau)\\ &\quad - 2P_3 S_{ky}S_{lz}A_2\sin(\pi J_{kl}t_1/2)\cos(\pi J_{kl}\tau)\\ &\quad + P_3 S_{lx}A_3\sin(\pi J_{kl}t_1/2)\sin(\pi J_{kl}\tau)\\ &\quad - 2P_3 S_{kz}S_{ly}A_3\cos(\pi J_{kl}t_1/2)\sin(\pi J_{kl}\tau)\\ &\quad - P_3 S_{ly}A_4\sin(\pi J_{kl}t_1/2)\sin(\pi J_{kl}\tau)\\ &\quad - 2P_3 S_{kz}S_{lx}A_4\cos(\pi J_{kl}t_1/2)\sin(\pi J_{kl}\tau)\\ &\quad + \text{Unobservable}\end{aligned} \tag{6}$$

The effective DDF becomes

$$\begin{aligned}B_d^{I_1\prime}(z) &= -\frac{1}{\gamma\tau_d}P_1\sin[(\omega_{I_1} + \gamma\Delta B(z))t_1/2 + \gamma G_2\delta z]\sin(H_1)\\ B_d^{I_2\prime}(z) &= \frac{2}{3}B_d^{I_1\prime}(z)\\ B_d^{S\prime}(z) &= \frac{2}{3}B_d^{I_1\prime}(z)\end{aligned} \tag{7}$$

We use $B_d^{I_1\prime}$, $B_d^{I_2\prime}$ and $B_d^{S\prime}$ to stand for $B_d^{I_1\prime}(z)$, $B_d^{I_2\prime}(z)$ and $B_d^{S\prime}(z)$ in the following expressions, respectively. The spins evolve under chemical shifts, J couplings, field inhomogeneities, the third gradient pulse, and the effective DDFs (ignoring the WS module) during the second $t_1/2$ period. Thus we have

$$\begin{aligned}\sigma^{I_1}(\tau+t_1,z) &= P_1 I_{1x}\cos(H_7)\sin(H_1)\cos(H_4) + P_1 I_{1y}\sin(H_7)\sin(H_1)\\ &\quad \cos(H_4) - P_1 I_{1y}\cos(H_7)\cos(H_1) + P_1 I_{1x}\sin(H_7)\cos(H_1)\\ \sigma^{I_2}(\tau+t_1,z) &= P_2 I_{2x}\cos\left[\gamma G_2\delta z + \left(\gamma B_d^{I_2\prime} - \gamma B_d^{I_2}\right)t_1/2\right]\sin(H_2)\\ &\quad + P_2 I_{2y}\sin\left[\gamma G_2\delta z + \left(\gamma B_d^{I_2\prime} - \gamma B_d^{I_2}\right)t_1/2\right]\sin(H_2)\\ \sigma^{S_k}(\tau+t_1,z) &= -P_3 S_{ky}B_1\cos(\pi J_{kl}\tau) + P_3 S_{lx}B_2\sin(\pi J_{kl}\tau)\\ &\quad - 2P_3 S_{kz}S_{ly}B_1\sin(\pi J_{kl}\tau) + 2P_3 S_{kx}S_{lz}B_2\cos(\pi J_{kl}\tau)\\ &\quad + P_3 S_{ly}B_3\sin(\pi J_{kl}\tau) + P_3 S_{kx}B_4\cos(\pi J_{kl}\tau)\\ &\quad + 2P_3 S_{ky}S_{lz}B_3\cos(\pi J_{kl}\tau) + 2P_3 S_{kz}S_{lx}B_4\sin(\pi J_{kl}\tau)\\ &\quad + \text{unobservable}\end{aligned} \tag{8}$$

where $H_7 = (\omega_{I_1} + \gamma\Delta B(z) + \gamma B_d^{I_1\prime})t_1/2 + 2\gamma G_2\delta z$, and

$$\begin{cases}B_1 = \cos\left[\gamma G_2\delta z + (\gamma B_d^{S\prime} - \gamma B_d^{S})t_1/2\right]\sin(H_3)\cos(\pi J_{kl}t_1)\\ B_2 = \cos\left[\gamma G_2\delta z + (\gamma B_d^{S\prime} - \gamma B_d^{S})t_1/2\right]\sin(H_3)\sin(\pi J_{kl}t_1)\\ B_3 = \sin\left[\gamma G_2\delta z + (\gamma B_d^{S\prime} - \gamma B_d^{S})t_1/2\right]\sin(H_3)\sin(\pi J_{kl}t_1)\\ B_4 = \sin\left[\gamma G_2\delta z + (\gamma B_d^{S\prime} - \gamma B_d^{S})t_1/2\right]\sin(H_3)\cos(\pi J_{kl}t_1)\end{cases}$$

During the acquisition period t_2, the observable transverse spin magnetizations evolve under chemical shifts, J coupling, field inhomogeneity, and effective DDFs. Since solvent signal would be efficiently suppressed by the WS module before acquisition, only the solute spin magnetizations are considered:

$$\begin{aligned}\sigma^{I_2}(\tau+t_1+t_2,z) &= P_2\sin(H_2)e^{iH_8}e^{i\left[\gamma B_d^{I_2\prime}(t_1/2+t_2)\right]}e^{-i\gamma B_d^{I_2}t_1/2}\\ \sigma^{S_k}(\tau+t_1+t_2,z) &= P_3\{-iC_1e^{iH_9} + C_2e^{iH_{10}}\}e^{i\left[\gamma B_d^{S\prime}(t_1/2+t_2)\right]}e^{-i\gamma B_d^{S}t_1/2},\end{aligned} \tag{9}$$

where

$$\begin{cases}H_8 = \omega_{I_2}t_2 + \gamma\Delta B(z)t_2 + \gamma G_2\delta z\\ H_9 = \omega_{S_k}t_2 + \gamma\Delta B(z)t_2 + \gamma G_2\delta z\\ H_{10} = \omega_{S_l}t_2 + \gamma\Delta B(z)t_2 + \gamma G_2\delta z\end{cases},$$

and $\begin{cases}C_1 = \cos[\pi J_{kl}(t_1+t_2)]\sin(H_3)\cos(\pi J_{kl}\tau)\\ C_2 = \sin[\pi J_{kl}(t_1+t_2)]\sin(H_3)\sin(\pi J_{kl}\tau)\end{cases}$.

Eq. (9) can be converted to [32]

$$\begin{aligned}\sigma^{I_2}(\tau+t_1+t_2,z) &= P_2\frac{e^{iH_2}}{2i}e^{iH_8}\sum_{m_1=-\infty}^{\infty}i^{m_1}J_{m_1}(P_1\xi_1)e^{im_1H_{11}}\\ &\quad \sum_{m_2=-\infty}^{\infty}i^{m_2}J_{m_2}(P_1\xi_2)e^{im_2H_{12}}\sum_{m_3=-\infty}^{\infty}i^{m_3}J_{m_3}(P_1\xi_3)e^{im_3H_1}\\ &\quad - P_2\frac{e^{-iH_2}}{2i}e^{iH_8}\sum_{m_1=-\infty}^{\infty}i^{m_1}J_{m_1}(P_1\xi_1)e^{im_1H_{11}}\\ &\quad \sum_{m_2=-\infty}^{\infty}i^{m_2}J_{m_2}(P_1\xi_2)e^{im_2H_{12}}\sum_{m_3=-\infty}^{\infty}i^{m_3}J_{m_3}(P_1\xi_3)e^{im_3H_1}\end{aligned}$$

$$\begin{aligned}\sigma^{S_k}(\tau+t_1+t_2,z) = &-iP_3D_1\cos(\pi J_{kl}\tau)\frac{e^{iH_3}}{2i}e^{iH_9}\\ &+iP_3D_1\cos(\pi J_{kl}\tau)\frac{e^{-iH_3}}{2i}e^{iH_9}\\ &+P_3D_2\sin(\pi J_{kl}\tau)\frac{e^{iH_3}}{2i}e^{iH_{10}}\\ &-P_3D_2\sin(\pi J_{kl}\tau)\frac{e^{-iH_3}}{2i}e^{iH_{10}}\end{aligned} \tag{10}$$

where $\begin{cases}H_{11}=\omega_{I_1}(t_1/2-\tau)+\gamma\Delta B(z)(t_1/2-\tau)+\gamma G_2\delta z-\gamma G_1\delta z\\ H_{12}=\omega_{I_1}(t_1/2+\tau)+\gamma\Delta B(z)(t_1/2+\tau)+\gamma G_2\delta z+\gamma G_1\delta z\end{cases}$, and

$$\begin{cases}D_1=\cos[\pi J_{kl}(t_1+t_2)]\sum\limits_{m_4=-\infty}^{\infty}i^{m_4}J_{m_4}(P_1\xi_4)e^{im_4H_{11}}\sum\limits_{m_5=-\infty}^{\infty}i^{m_5}J_{m_5}(P_1\xi_5)e^{im_5H_{12}}\sum\limits_{m_6=-\infty}^{\infty}i^{m_6}J_{m_6}(P_1\xi_6)e^{im_6H_1}\\ D_2=\sin[\pi J_{kl}(t_1+t_2)]\sum\limits_{m_4=-\infty}^{\infty}i^{m_4}J_{m_4}(P_1\xi_4)e^{im_4H_{11}}\sum\limits_{m_5=-\infty}^{\infty}i^{m_5}J_{m_5}(P_1\xi_5)e^{im_5H_{12}}\sum\limits_{m_6=-\infty}^{\infty}i^{m_6}J_{m_6}(P_1\xi_6)e^{im_6H_1}\end{cases},$$

in which $J_{m_1}(\xi_1)$,$J_{m_2}(\xi_2)$,$J_{m_3}(\xi_3)$,$J_{m_4}(\xi_4)$,$J_{m_5}(\xi_5)$ and $J_{m_6}(\xi_6)$ are the Bessel functions with integer orders m_1, m_2, m_3, m_4, m_5 and m_6 respectively; and $\xi_1=\xi_4=-\frac{1}{3\tau_d}(t_1/2+t_2)$, $\xi_2=\xi_5=-\xi_1$, and $\xi_3=\xi_6=\frac{t_1}{3\tau_d}$. In order to evaluate the detectable signals from the whole sample, an average of the complex magnetization over all z positions should be taken. For Eq. (10), if the sample size is much larger than the dipolar correlation distance (typically around 100 μm), only several terms can survive after the spatial averaging across the sample:

$$\begin{aligned}\sigma^{I_2}(\tau+t_1+t_2,z)&=P_1P_2\Psi_{I_2}\\ \sigma^{S_k}(\tau+t_1+t_2,z)&=P_1P_3\Psi_{S_k}\end{aligned} \tag{11}$$

where E_1, E_2, E_3, E_4, Ψ_{I_2} and Ψ_{S_k} are

$$\begin{aligned}E_1&=J_0(\xi_1)J_0(\xi_3)J_{-1}(\xi_1)\cos(\pi J_{kl}\tau)e^{i(\omega_{S_k}-\omega_{I_1})\tau}\\ E_2&=J_0(\xi_1)J_0(\xi_3)J_{-1}(\xi_1)\cos(\pi J_{kl}\tau)e^{i(\omega_{I_1}-\omega_{S_k})\tau}\\ E_3&=J_0(\xi_1)J_0(\xi_3)J_{-1}(\xi_1)\sin((\pi J_{kl}\tau)e^{i(\omega_{S_k}-\omega_{I_1})\tau}\\ E_4&=J_0(\xi_1)J_0(\xi_3)J_{-1}(\xi_1)\sin((\pi J_{kl}\tau)e^{i(\omega_{I_1}-\omega_{S_k})\tau}\\ \Psi_{I_2}&=\tfrac{1}{2}J_0(\xi_3)J_0(\xi_1)J_{-1}(\xi_1)e^{i(\omega_{I_2}-\omega_{I_1})\tau}e^{-i(\omega_{I_1}+\gamma\Delta B(z))t_1/2}e^{i(\omega_{I_2}+\gamma\Delta B(z))t_2}\\ &\quad+\tfrac{1}{2}J_0(\xi_3)J_0(\xi_2)J_{-1}(\xi_1)e^{-i(\omega_{I_2}-\omega_{I_1})\tau}e^{-i(\omega_{I_1}+\gamma\Delta B(z))t_1/2}e^{i(\omega_{I_2}+\gamma\Delta B(z))t_2}\\ \Psi_{S_k}&=-\tfrac{i}{4}(E_1+E_2)e^{-i(\omega_{I_1}+\gamma\Delta B(z)-2\pi J_{kl})t_1/2}e^{i(\omega_{S_k}+\gamma\Delta B(z)+\pi J_{kl})t_2}\\ &\quad-\tfrac{i}{4}(E_1+E_2)e^{-i(\omega_{I_1}+\gamma\Delta B(z)+2\pi J_{kl})t_1/2}e^{i(\omega_{S_k}+\gamma\Delta B(z)-\pi J_{kl})t_2}\\ &\quad+\tfrac{1}{4}(E_3+E_4)e^{-i(\omega_{I_1}+\gamma\Delta B(z)-2\pi J_{kl})t_1/2}e^{i(\omega_{S_l}+\gamma\Delta B(z)+\pi J_{kl})t_2}\\ &\quad-\tfrac{1}{4}(E_4+E_3)e^{-i(\omega_{I_1}+\gamma\Delta B(z)+2\pi J_{kl})t_1/2}e^{i(\omega_{S_l}+\gamma\Delta B(z)-\pi J_{kl})t_2}\end{aligned}$$

Eq. (11) shows that there are three peaks locating at $(\gamma\Delta B(z)/2,\omega_{I_2}+\gamma\Delta B(z))$, $((\gamma\Delta B(z)\pm 2\pi J_{kl})/2,\omega_{S_k}+\gamma\Delta B(z)\pm\pi J_{kl})$ and $((\gamma\Delta B(z)\pm 2\pi J_{kl})/2,\omega_{S_l}+\gamma\Delta B(z)\pm\pi J_{kl})$ when the spectrometer reference frequency is set to $\omega_{I_1}(\omega_{I_1}=0)$. Consider the whole spin system, there would be three peaks centering at $\omega_{I_2},\omega_{S_k}$ and ω_{S_l} in the t_2 dimension, and 0 Hz in t_1 dimension. The direction of the inhomogeneous broadenings with respect to F1 axis is along the angle of arctan(2) = 63.4° and the ratio of the projection lengths of every streak in the F1 and F2 dimensions is 1:2. However, the projection onto the F2 dimension after rotating the streaks by 63.4° counterclockwise would give a 1D high-resolution spectrum. The J coupling constants are magnified by three times [21]. From above analysis, we can see that the resulted 2D spectra have similar characters as previous 2D IDEAL-II spectra except for the phase and amplitude of signals [21].

By encoding the amplitude and phase of individual frequency component according to every row of the four order Hadamard matrix, four soft polychromatic pulses can be produced accordingly (see below). Performing four scans respectively, we get four 2D FIDs.

	I_1	S_k	I_2	S_l	
scan 1	+1	+1	+1	+1	first soft pulse
scan 2	+1	+1	−1	−1	second soft pulse
scan 3	+1	−1	+1	−1	third soft pulse
scan 4	+1	−1	−1	+1	fourth soft pulse

In every 2D FID, the signal can be described as $P_1P_2\cdot\Psi_{I_2}+P_1P_3\cdot\Psi_{S_k}+P_1P_4\cdot\Psi_{S_l}$. It comes from all frequency-bearing areas except for the solvent spin which is suppressed by the WS module. After decoding the detected signals, the signals from every frequency site will be separated and given by $4\Psi_{I_2}$, $4\Psi_{S_k}$ and $4\Psi_{S_l}$ when the solvent frequency site in every soft polychromatic pulse is encoded by the first column of the above Hadamard matrix, i.e. P_1 is '+'. After Fourier transformation, the decoded signals produce three 2D spectra. Rotating the three 2D spectra by 63.4° counterclockwise and then projecting onto the F2 dimension, three 1D high-resolution spectra can be obtained, which hold all useful correlation information for the 2D COSY spectrum based on the symmetrical characteristic.

3. Materials and methods

All experiments were performed at 298 K on a Varian NMR System 500 MHz spectrometer equipped with a 5 mm ^{1}H {^{15}N–31P} XYZ indirect detection probe. Firstly, a dilute solution of ethyl acetate, acetone in dichloromethane was studied in an intentionally deshimmed inhomogeneous field (75 Hz linewidth). The molar ratio of acetone:ethyl acetate:dichloromethane was about 1:1.6:300. For the proposed sequence, an eight order Hadamard matrix was used since there were five peaks for the sample. The selective $\pi/2$ Gaussian pulse only acted on dichloromethane. The duration of polychromatic pulse was 100 ms to give a relatively narrow excitation bandwidth for the single radiofrequency channel of polychromatic pulse. To suppress the strong signal of dichloromethane, the W3 binomial π pulse was used as the solvent-exclusive π pulse in the WS module [33]. The pulse repetition time was 3.1 s, and the acquisition time t_2 was 0.2 s. 21 × 1042 points were acquired with spectral widths of 70 Hz × 5200 Hz (F1 × F2) in about 1 min. The time for complete a Hadamard-IDEAL-II acquisition was about 10 min.

For comparison, conventional COSY experiments were also performed in the same inhomogeneous field and a well-shimmed field. The pulse repetition time was 1.5 s, and the acquisition time t_2 was 1 s. To get a high precision 2D COSY spectrum, 2500 × 5208 points were acquired with spectral widths of 5200 Hz in both F1 and F2 dimensions. A four-step phase cycling scheme with the phases of the first non-selective pulse (π, π, $3\pi/2$, $3\pi/2$), the phases of the second non-selective pulse (0, $\pi/2$, $3\pi/2$, 0) and the phases of the receiver (π, 0, $3\pi/2$, $\pi/2$) was employed.

To further verify the theoretical predictions and experimental results of the new sequence, simulation was performed on the

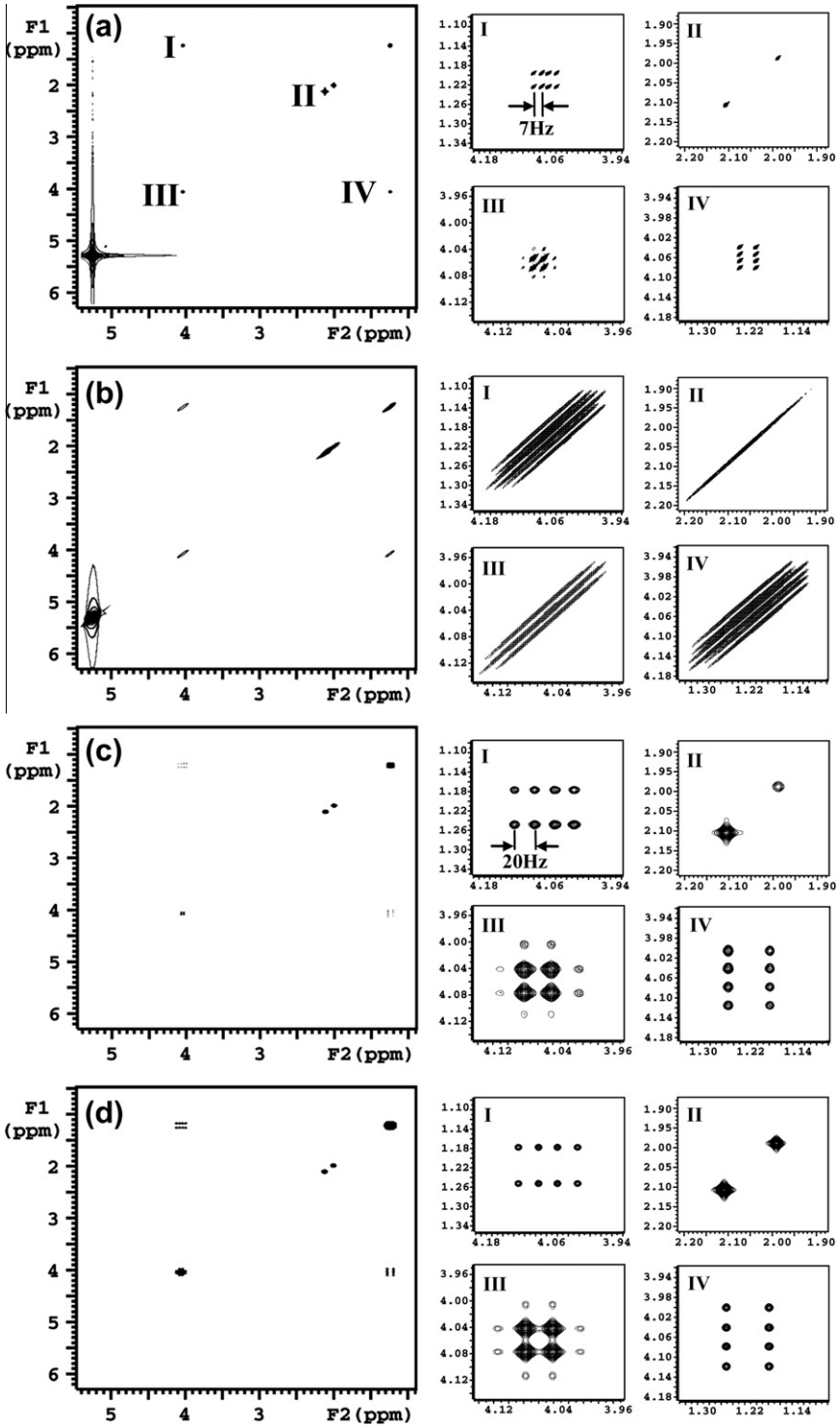

Fig. 3. Experimental (a–c) and simulated (d) 2D COSY spectra of the sample of ethyl acetate and acetone dissolved in dichloromethane. (a) Conventional spectrum obtained in a well-shimmed field, (b) conventional spectrum obtained in an inhomogeneous field, (c) Hadamard-IDEAL-II spectrum obtained in the same inhomogeneous field as (b), and (d) simulated Hadamard-IDEAL-II spectrum obtained in an inhomogeneous field similar to (b). The regions labeled as (I), (II), (III), and (IV) were expanded for comparison.

same sample with the program package developed by our research group on a personal computer (Intel Core 2 Q6600, 2 Gb memories) [34]. The parameters for simulation were set as close to the experimental parameters as possible. The background field was set to 75 Hz linewidth.

In addition, a sample of 1-bromobutane and 4-bromoanisole dissolved in dichloromethane was utilized to testify the feasibility of our sequence for complicated spin systems. Similar to the first sample, two COSY spectra were obtained with the Hadamard-IDEAL-II and conventional COSY sequences respectively in a same inhomogeneous field (106 Hz linewidth), together with a conventional COSY spectrum acquired in a well-shimmed field. For the Hadamard-IDEAL-II, the pulse repetition time was 3.0 s. The acquisition time t_2 was 0.2 s. 24 × 1000 points were acquired with spectral widths of 100 Hz × 5000 Hz (F1 × F2). For the conventional COSY, the pulse repetition time was 1.5 s and the acquisition time was 1 s. The spectral width was 5200 Hz in both F1 and F2 dimensions. All other parameters and phase cycling scheme were set the

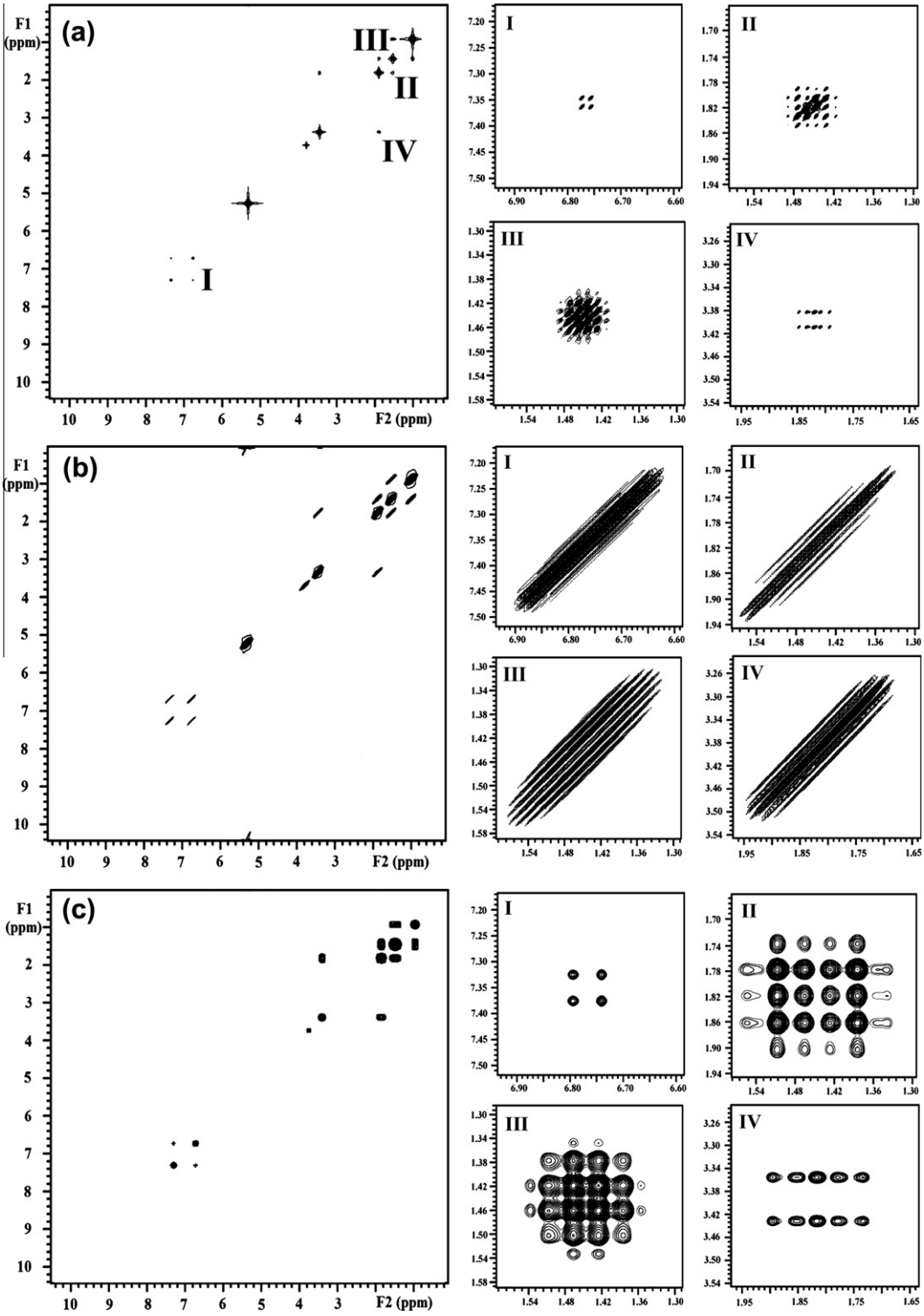

Fig. 4. Experimental 2D COSY spectra of the sample of 1-bromobutane and 4-bromoanisole dissolved in dichloromethane. (a) Conventional spectrum obtained in a well-shimmed field, (b) conventional spectrum obtained in an inhomogeneous field, and (c) Hadamard-IDEAL-II spectrum obtained in the same inhomogeneous field as (b). The regions labeled as (I), (II), (III), and (IV) were expanded for comparison.

same as those for the first sample. The total acquisition time for a Hadamard-encoded COSY spectrum was about 10 min.

4. Experimental results and discussion

The experimental and the simulated results of the mixture of ethyl acetate, acetone and dichloromethane are shown in Fig. 3. The conventional high-resolution 2D COSY spectrum in a well-shimmed field is presented in Fig. 3a. The 2D COSY spectra acquired in the inhomogeneous field with the conventional and Hadamard-IDEAL-II pulse sequences are given in Fig. 3b and c, respectively. The simulated spectrum is shown in Fig. 3d. The diagonal and cross peaks were amplified for clear comparison. The simulation result is in good agreement with the experimental one. In

the conventional 2D COSY sequence, the coherence orders are +1 and −1 in the t_1 and t_2 periods, respectively, which are sensitive to the field inhomogeneity. The inhomogeneous field results in inhomogeneous broadenings (see Fig. 3b). Since the inhomogeneous broadening is along the diagonal direction, two neighboring diagonal peaks around 2.1 ppm are partly overlapped (region II of Fig. 3b). In addition, the *J* coupling splitting is not easy to identify. The IDEAL-II sequence can yield the 1D high-resolution spectra in inhomogeneous fields, which supply high-resolution information for reconstructing 2D COSY spectrum by Hadamard encoding and decoding techniques. The reconstructed spectra shown in Fig. 3c and d hold well resolution in contrast with the one obtained under homogeneous field from the conventional COSY method (see Fig. 3a). The signal of dichloromethane (at 5.3 ppm) is well suppressed. The *J* coupling constants in the Hadamard-IDEAL-II spectrum are scaled to three times of those in the conventional COSY spectrum (20 Hz *vs.* 7 Hz, as indicated in Fig. 3), which is helpful for weakly-coupled spin systems, but may bring trouble for strongly-coupled spin systems. Note that the two singlets in region II that are overlapped in the conventional COSY spectrum under the inhomogeneous field are now correctly separated in Fig. 3c and d. This indicates that the new method is valid even when the field inhomogeneity is large enough to make the neighboring peaks overlapped. Under this case, the interested frequency sites may not be determined directly, thus an extra 2D IDEAL-II spectrum should be acquired to provide a high-resolution 1D spectrum to decide the correct frequency sites. The extra experiment can be obtained within less than 1 min. It should be noted that if the overlap between neighboring peaks is serious due to the inhomogeneous field, and the excitation bandwidth of the single radiofrequency channel of polychromatic pulse is not narrow enough, there will be not only one resonance inside the single radiofrequency channel. In such case, artificial peaks will appear. However, the artificial peaks are not exactly at the positions of cross-peaks of two overlapped peaks since the excited frequency in the overlapped region for a specific spin is deviated from its Lamor frequency due to inhomogeneous field. Therefore, correct spectral information can still be obtained provided that the artificial peaks can be distinguished. The results also show that the present method is applicable to relatively dilute solutions in inhomogeneous fields.

The experimental results of the sample of 1-bromobutane and 4-bromoanisole in dichloromethane are illustrated in Fig. 4. The 2D COSY spectra acquired with the conventional method in the well-shimmed and deshimmed fields are shown in Fig. 4a and b, respectively. The reconstructed COSY spectrum from the new sequence is shown in Fig. 4c. Four regions expanded for details are labeled as I, II, III, and IV. It can be seen that the high-resolution COSY spectrum obtained with the proposed method in Fig. 4c is similar to the conventional high-resolution COSY spectrum in Fig. 4a, except that the apparent *J* coupling constants are threefold magnified.

5. Conclusions

A fast acquisition sequence, Hadamard-IDEAL-II, was designed to obtain high-resolution 2D COSY spectra in inhomogeneous fields. Theoretical analysis, experimental measurements, and computer simulations show that the new sequence can be applied to achieve high-resolution 2D COSY spectra. The new sequence can not only recover spectral information concealed by inhomogeneous broadenings, but also greatly shorten the acquisition time. The 2D reconstructed COSY spectrum is free of inhomogeneous effects and preserves all useful information. The acquisition time is in the order of minutes. The method proposed herein may be applicable to time-concerned high-resolution experiments in inhomogeneous fields. The feature that the homo-nuclear *J*-couplings is scaled by a factor of three points to potential increase in signal overlap and reduction in resolution. However, in certain situations increased *J*-coupling resolution can also be a useful feature, such as in the detection of weekly-coupled spin systems.

Acknowledgments

This work was partially supported by the NNSF of China under Grants 10974164 and 10875101, the Fundamental Research Funds for the Central Universities under Grant 2010121101, and NSF of Fujian Province of China under Grant 2009J05087.

References

[1] A. Spyros, D. Anglos, Study of aging in oil paintings by 1D and 2D NMR spectroscopy, Anal. Chem. 76 (2004) 4929–4936.
[2] T. Ye, H. Mo, N. Shanaiah, G.A. Gowda, S.C. Zhang, D. Raftery, Chemoselective ^{15}N tag for sensitive and high-resolution nuclear magnetic resonance profiling of the carboxyl-containing metabolome, Anal. Chem. 81 (2009) 4882–4888.
[3] S.G. Köneke, J.D. van Beek, M. Ernst, B.H. Meier, Characteristics of zero-quantum correlation spectroscopy in MAS NMR experiments, J. Magn. Reson. 207 (2010) 197–205.
[4] C. Faber, E. Pracht, A. Haase, Resolution enhancement in in vivo NMR spectroscopy: detection of intermolecular zero-quantum coherences, J. Magn. Reson. 161 (2003) 265–274.
[5] M.J. Lin, X. Chen, S.H. Cai, Z. Chen, High-resolution magnetic resonance spectroscopy in unstable fields via intermolecular zero-quantum coherences, Phys. Chem. Chem. Phys. 12 (2010) 6014–6020.
[6] G. Galiana, R.T. Branca, E.R. Jenista, W.S. Warren, Accurate temperature imaging based on intermolecular coherences in magnetic resonance, Science 322 (2008) 421–424.
[7] W. Barros, D.F. Gochberg, J.C. Gore, Assessing signal enhancement in distant dipolar field-based sequences, J. Magn. Reson. 189 (2007) 2–37.
[8] W. Barros, J.C. Gore, D.F. Gochberg, Simultaneous measurement of D and T2 using the distant dipolar field, J. Magn. Reson. 178 (2006) 166–169.
[9] L.S. Bouchard, W.S. Warren, Multiple-quantum vector field imaging by magnetic resonance, J. Magn. Reson. 177 (2005) 9–21.
[10] S. Datta, S.Y. Huang, Y.Y. Lin, Contrast enhancement by feedback fields in magnetic resonance imaging, J. Phys. Chem. B 110 (2006) 22071–22078.
[11] A. Schäfer, H.E. Möller, Functional contrast based on intermolecular double-quantum coherences: influence of the correlation distance, Magn. Reson. Med. 58 (2007) 696–704.
[12] V. Hoerr, A. Purea, C. Faber, NMR separation of intra- and extracellular compounds based on intermolecular coherences, Biophys. J. 99 (2010) 2336–2343.
[13] W.S. Warren, W. Richter, A.H. Andreotti, Generation of impossible cross-peaks between bulk water and biomolecules in solution NMR, Science 262 (1993) 2005–2009.
[14] Z. Chen, Z.W. Chen, J.H. Zhong, High-resolution NMR spectra in inhomogeneous fields via IDEAL (Intermolecular Dipolar-Interaction Enhanced All Lines) method, J. Am. Chem. Soc. 126 (2004) 446–447.
[15] C.B. Cai, Y.Q. Lin, S.H. Cai, Z. Chen, J.H. Zhong, High-resolution NMR spectra in inhomogeneous fields utilizing the CRAZED sequence without coherence selection gradients, J. Magn. Reson. 193 (2008) 94–101.
[16] L.S. Bouchard, R.R. Rizi, W.S. Warren, Magnetization structure contrast based on intermolecular multiple-quantum coherences, Magn. Reson. Med. 48 (2002) 973–979.
[17] Y.Q. Huang, X. Chen, S.H. Cai, C.B. Cai, Z. Chen, High-resolution two-dimensional correlation spectroscopy in inhomogeneous fields: new application of intermolecular zero-quantum coherences, J. Chem. Phys. 132 (2010) 34507.
[18] M.J. Lin, Y.Q. Huang, X. Chen, S.H. Cai, Z. Chen, High-resolution 2D NMR spectra in inhomogeneous fields based on intermolecular multiple-quantum coherences with efficient acquisition schemes, J. Magn. Reson. 208 (2011) 87–94.
[19] E. Kupče, R. Freeman, Two-dimensional Hadamard spectroscopy, J. Magn. Reson. 162 (2003) 300–310.
[20] K.W. Eberhardt, C.L. Degen, B.H. Meier, Fast magnetic resonance force microscopy with Hadamard encoding, Phys. Rev. B 76 (2007) 180405.
[21] Z. Chen, S.H. Cai, Z.W. Chen, J.H. Zhong, Fast acquisition of high-resolution NMR spectra in inhomogeneous fields via intermolecular double-quantum coherences, J. Chem. Phys. 130 (2009) 084504.
[22] E. Kupče, R. Freeman, Molecular structure from a single NMR sequence (fast-PANACEA), J. Magn. Reson. 206 (2010) 47–153.
[23] S.L. Patt, Single- and multiple-frequency-shifted laminar pulses, J. Magn. Reson. 96 (1992) 94–102.
[24] E. Kupče, T. Nishida, R. Freeman, Hadamard NMR spectroscopy, Prog. Nucl. Mag. Reson. Spectrosc. 42 (2003) 95–122.
[25] T.L. Hwang, A.J. Shaka, Water suppression that works. Excitation sculpting using arbitrary waveforms and pulsed field gradients, J. Magn. Reson. 112 (1995) 275–279.

[26] J. Jeener, A. Vlassenbroek, P. Broekaert, Unified derivation of the dipolar field and relaxation terms in the Bloch–Redfield equations of liquid NMR, J. Chem. Phys. 103 (1995) 1309–1332.
[27] R. Bowtell, R.M. Bowley, P. Glover, Multiple spin echoes in liquids in a high magnetic-field, J. Magn. Reson. 88 (1990) 643–651.
[28] G. Deville, M. Bernier, J.M. Delrieux, NMR multiple echoes observed in solid ^{3}He, Phys. Rev. B 19 (1979) 5666–5688.
[29] W. Barros, D.F. Gochberg, J.C. Gore, Nuclear magnetic resonance signal dynamics of liquids in the presence of distant dipolar fields, revisited, J. Chem. Phys. 130 (2009) 174506.
[30] C. Faber, C. Heil, B. Zahneisen, D.Z. Balla, R. Bowtell, Sensitivity to local dipole fields in the CRAZED experiment: an approach to bright spot MRI, J. Magn. Reson. 182 (2006) 315–324.
[31] T. Enss, S. Ahn, W.S. Warren, Visualizing the dipolar field in solution NMR and MR imaging: three-dimensional structure simulations, Chem. Phys. Lett. 305 (1999) 101–108.
[32] P.M. Morse, H. Feshbach, Methods of Theoretical Physics, McGraw-Hill, New York, 1953.
[33] V. Sklenar, M. Piotto, R. Leppik, V. Saudek, Gradient-tailored water suppression for ^{1}H–^{15}N HSQC experiments optimized to retain full sensitivity, J. Magn. Reson. A 102 (1993) 241–245.
[34] C.B. Cai, M.J. Lin, Z. Chen, X. Chen, S.H. Cai, J.H. Zhong, SPROM – an efficient program for NMR/MRI simulations of inter- and intra-molecular multiple quantum coherences, C. R. Physique 9 (2008) 119–126.